Feasibility study for joint retrieval of air density and ozone concentration profiles in the mesosphere using an ultraviolet limb-scan technique*

GUO Xia[1 **], LU Yao[1, 2] and LÜ Daren[1]

(1. LAGEO, Institute of Atmospheric Physics, Chinese Academy of Sciences, Beijing 100029, China; 2. Department of Physics, Beijing University of Science and Technology, Beijing 100081, China)

Received May 13, 2003; revised July 9, 2003

Abstract For joint retrieval of vertical distributions of both air density and ozone concentration in the mesosphere which are two of the most important atmospheric parameters in this region, a retrieval scheme is suggested by using satellite limb scan observation at two UV wavelengths, i.e. 255 nm and 296 nm. The retrieval scheme is the modification of the direct method by Aruga and Heath with two UV wavelengths and two atmospheric parameters. Feasibility study was made based on simulated limb scan radiances computed with a single scattering radiative transfer algorithms of spherical geometry developed by the present authors and the inversion technique. Results of the simulations show that it is feasible to retrieve air density and ozone concentration vertical distributions on a global basis from satellite UV limb scan over the altitude range of 50 km ~ 100 km with a vertical resolution of 1 km. The errors of the inferred profiles by using the joint inversion algorithm are greatly deduced, especially in the upper-mesosphere heights, compared with those by using the single inversion technique with a single wavelength.

Keywords: mesosphere, air density and ozone concentration, ultraviolet limb-scan technique.

Recently it has been recognized that the coupling and interactions between the upper and the lower atmosphere play important roles in both earth climate and also the space weather. It is known that global warming on the earth surface and in the troposphere resulting from the increasing of green house gas emission by human activities may be accompanied with global cooling in the stratosphere and the mesosphere. On the other hand, solar activities and the corresponding strong space weather events may also influence the earth climate through the interference of the upper and middle atmosphere. The mechanisms for this coupling are multiple, including dynamical, thermo-dynamical, radiative, chemical and those which are not well-known. To clearly understand those processes and mechanisms, global and continuous monitoring of atmospheric parameters is necessary. In the previous decades, a series of monitoring efforts by ground-based remote sensing techniques, including the mesosphere-stratosphere-troposphere (MST) radar, Rayleigh lidar and Sodium lidar, etc. have been made to reveal the dynamic structure of the middle-upper atmosphere, in particular the mesospheric gravity waves (GW) induced by the upward propagation of GW originated in the lower atmosphere. In the meantime, satellite monitoring of the middle and upper atmosphere structure and constituents was conducted with research satellites, such as the upper atmosphere research satellite (UARS).

Satellite remote sensing has played an important role in the global monitoring of the middle atmosphere. A plenty of work about the dynamical, thermal and constituent remote sensing in the stratosphere has been carried out. In contrast, less work has been done for the remote sensing of the mesosphere. Only when the achievement of the temporal and spatial distributions of air density and ozone concentration with a high resolution has been made simultaneously could we understand correctly the processes and mechanisms in the mesosphere.

Up to now, little work has been done on the joint retrieval of air density and ozone concentration distributions while a great deal of research work on ozone concentration retrieval has been done by using ultraviolet remote sensing. During the past decades, total ozone amount and vertical distribution have been obtained from satellite observations using UV, visible, IR techniques. These methods have been used to

* Supported by the National Natural Science Foundation of China (Grant No. 40075007)

** To whom correspondence should be addressed. E-mail: guoxia@mail.iap.ac.cn

derive total ozone amount or its vertical distribution by using an observational technique in which the detector views the subsatellite point on the earth. The backscattered ultraviolet technique for viewing ozone concentration provides a limited resolution, approximately 10 km, and is only effective at an altitude higher than the altitude of the ozone concentration peak, i.e. 23 km[1]. Occultation measurements give an excellent vertical resolution, but with a limitation of satellite viewing sunrise/sunset latitudes. The need for high resolution measurements of the vertical distribution of ozone concentration on a global basis has led to the development of atmospheric limb-scan technique. Limb scanning gives vertical resolution which is comparable to the occultation measurements such as the stratospheric aerosol and gas experiment (SAGE) and the global coverage similar to the solar backscatter ultraviolet (SBUV) instrument. An advantage of limb-scan technique using solar UV radiation is that the limb scan is possible for any solar illuminated azimuth angle. Rusch et al.[2] retrieved ozone concentration between 48 ~ 68 km by an ultraviolet spectrometer onboard the Solar Mesosphere Explorer satellite launched in October 1981[3~7]. Some research work on the retrieval of ozone concentration profiles has been carried out since November, 1997 by the instruments SOLSE/LORE flown on the Shuttle Flight STS-87 with a high spatial and spectral resolution in the height range of 25 km ~ 55 km[8,9]. However their results have a limited inversion precision of ozone concentration. The uncertainty of air density profiles is one of the important factors influencing the retrieval accuracy.

In the present paper, a method for retrieval of air density and ozone concentration profiles by satellite observed solar UV limb radiances of multiple heights is described in terms of the inversion technique similar to Aruga and Heath[10,11], referred to as the "Direct Method". The inversion equation for this joint inversion method is based on weighting functions which correspond to the sensitivities of the limb radiances to the relative increment of air density and ozone concentration separately at each altitude. The equation is solved by an iteration technique similar to the Direct Method. Due to the lack of real UV limb-scan data of 1 km height resolution, we carried out the feasibility study by numerical simulations which were conducted with the wavelengths of 255 nm and 296 nm. The simulation results reveal the feasibility of determining air density and ozone concentration profiles on a global basis from satellite platforms over the altitude range of 50 km ~ 100 km with a vertical resolution of 1 km. The inferred profile errors using the joint inversion algorithm are greatly deduced, especially at the upper-mesosphere heights compared with those using the single inversion technique with a single wavelength.

1 Principle of the inversion method

1.1 Radiative theory

The detector on the spacecraft views the atmosphere limb with an extremely small field of view and scans vertically along the tangent ray height as shown in Fig. 1. The radiative intensity of satellite limb scanning can be obtained with a single scattering radiative transfer algorithm in spherically layered atmosphere when the air density and ozone concentration profile are known. It is assumed that the effects of uncertainties at spacecraft altitude are negligible. The effects of refraction along the line of sight are also negligible in the upper atmosphere. We assume that the atmosphere consists of only air molecules and ozone, thus only Rayleigh scattering and ozone absorption are taken into account. As other minor constituents in radiative transfer can be neglected in these wavelengths, this simplification is of high accuracy.

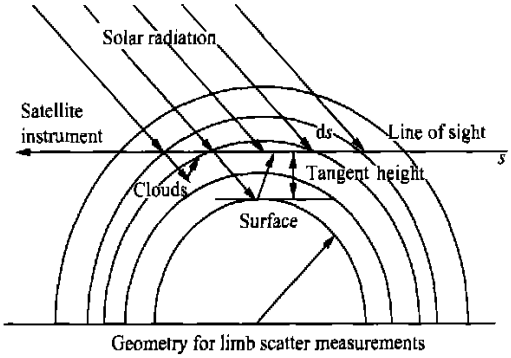

Geometry for limb scatter measurements
Fig. 1. Map of limb scattering.

1.2 Determination of the vertical distributions of air density and ozone

1.2.1 Inversion method. In this section, we propose a method of determining the vertical distributions of air density $N_{air}(x)$ and ozone concentration $N_{O_3}(x)$. Consider a set of m tangent heights l_1, l_2, …, l_m and define F_i for the ith tangent height as follows:

$$F_i = I(l_i) - I(l_i), \quad i = 1, 2, \cdots, m, \quad (1)$$

where $I(l_i)$ is the scattered intensity calculated for a tangent height of l_i and with the predetermined air density and ozone concentration distributions $(N_{air}(x), N_{O_3}(x))$, and $I(l_i)$ is the measured intensity with the real atmosphere distributions $(N_{air}(x), N_{O_3}(x))$. Here, we divide the whole atmosphere into n layers and define $(N_{air}(x), N_{O_3}(x))$ and $(\bar{N}_{air}(x), \bar{N}_{O_3}(x))$ to be the average number densities in the jth layer for the actual and pre-determined distributions respectively. We define y_j, z_j for the jth layer as follows:

$$\begin{aligned} y_j &= (N_{O_3}(j) - \bar{N}_{O_3}(j))/\bar{N}_{O_3}(j), \\ z_j &= (N_{air}(j) - \bar{N}_{air}(j))/\bar{N}_{air}(j), \end{aligned} \tag{2}$$

$$\begin{aligned} \bar{N}_{O_3}[j] &= \bar{N}_{O_3}(j)(1+y_j), \\ \bar{N}_{air}[j] &= \bar{N}_{air}(j)(1+z_j), \quad j = 1, 2, \cdots, n. \end{aligned} \tag{3}$$

Define $N^*_{air}(j)$ as a distribution in which the air number density is $N_{air}(j)$ only at the jth layer and $\bar{N}_{air}(j)$ in other layers. $N^*_{O_3}(j)$ is defined similar to $N^*_{air}(j)$.

$$\begin{cases} N^*_{air}[j] = \begin{cases} \bar{N}_{air}(x), & x < x_{j-1},\ x > x_j, \\ N_{air}(x) \cong \bar{N}_{air}(x)\cdot(1+z_j), & x_{j-1} \leqslant x \leqslant x_j, \end{cases} \\ j = 1, 2, \cdots, n, \\ N^*_{O_3}[j] = \begin{cases} \bar{N}_{O_3}(x), & x < x_{j-1},\ x > x_j, \\ N_{O_3}(x) \cong \bar{N}_{O_3}(x)\cdot(1+y_j), & x_{j-1} \leqslant x \leqslant x_j, \end{cases} \\ j = 1, 2, \cdots, n. \end{cases} \tag{4}$$

Here we consider the difference between the intensities $I^*(l_i, y_j, z_j)$, $I(l_i)$ and denote it by $F_i(0, \cdots, y_j, z_j, \cdots, 0)$ or simply by $F_j(y_j, z_j)$. The following alternate equations are obtained.

$$\begin{aligned} F_i(y_j, z_j) &= F_i(0, 0, \cdots, y_j, z_j, \cdots, 0, 0) \\ &= I^*(l_i, y_j, z_j) - I(l_i), \\ F_i(0) &= F(0, 0, \cdots, 0, 0, \cdots, 0, 0) \\ &= I^*(l_i, 0, 0) - I(l_i), \end{aligned} \tag{5}$$

$$\begin{aligned} F_i(y_1, z_1) &= F(y_1, z_1, 0, 0, \cdots, 0, 0), \\ F_i(y_2, z_2) &= F(0, 0, y_2, z_2, 0, 0, \cdots, 0, 0), \\ &\vdots \qquad\qquad \vdots \\ F_i(y_n, z_n) &= F(0, 0, \cdots, 0, 0, y_n, z_n). \end{aligned} \tag{6}$$

The quantity F_i defined in Eq. (1) can be expressed as

$$\begin{aligned} F_i &= F_i(y_1, z_1, y_2, z_2, \cdots, y_n, z_n), \\ & i = 1, 2, \cdots, m. \end{aligned} \tag{7}$$

The sum $\sum_{j=1}^{n} F_i(y_j, z_j)$ is approximately equal to $F_i(y_1, z_1, y_2, z_2, \cdots, y_n, z_n)$ if (y_j, z_j) is small, but these two are not exactly equal. Therefore, we equate them by introducing the multiplication factor of ε_i as below:

$$\begin{aligned} F_i &= F_i(y_1, z_1, y_2, z_2, \cdots, y_n, z_n) \\ &= \left[\sum_{j=1}^{n} F_i(y_j, z_j)\right] \varepsilon_i, \end{aligned} \tag{8}$$

The factor ε_i is nearly equal to 1.0 as long as the actual distribution does not far depart from the predetermined distribution. For small values of (y_j, z_j), taking the first order of approximation in Taylor expansion for Eq. (8), the following equation is obtained:

$$\begin{aligned} F_i(y_j, z_j) = &\left[\frac{\partial F_i(y_j, z_j)}{\partial y_j}\right]_{y_j=0} y_j \\ &+ \left[\frac{\partial F_i(y_j, z_j)}{\partial z_j}\right]_{z_j=0} z_j. \end{aligned} \tag{9}$$

Define the differential coefficients (D_{ij}, E_{ij}) by

$$\begin{aligned} D_{ij} &= \left[\frac{\partial F_i(y_j, z_j)}{\partial y_j}\right]_{y_j=0}, \\ E_{ij} &= \left[\frac{\partial F_i(y_j, z_j)}{\partial z_j}\right]_{z_j=0}, \\ & i = 1, 2, \cdots, m, \quad j = 1, 2, \cdots, n, \end{aligned} \tag{10}$$

and from Eqs. (3 ~ 10), we obtain

$$\begin{aligned} D_{ij} &= \frac{F_i\left(0, 0, \cdots, \frac{\Delta y_j}{2}, 0, \cdots, 0, 0\right) - F_i\left(0, 0, \cdots, \frac{-\Delta y_j}{2}, 0, \cdots, 0, 0\right)}{\Delta y_j} \\ &= \frac{I^*\left(l_i, \frac{\Delta y_j}{2}, 0\right) - I^*\left(l_i, \frac{-\Delta y_j}{2}, 0\right)}{\Delta y_j}, \end{aligned} \tag{11a}$$

$$E_{ij} = \frac{F_i\left(0, 0, \cdots, \frac{\Delta z_j}{2}, 0, \cdots, 0, 0\right) - F_i\left(0, 0, \cdots, \frac{-\Delta z_j}{2}, 0, \cdots, 0, 0\right)}{\Delta z_j}$$

$$= \frac{I^*\left(l_i, 0, \frac{\Delta z_j}{2}\right) - I^*\left(l_i, 0, \frac{-\Delta z_j}{2}\right)}{\Delta z_j}, \tag{11b}$$

where $I^*(l_i, \pm y_j/2, 0)$, $I^*(l_i, 0, \pm z_j/2)$ are the intensities of the scattered radiation computed for the air density and ozone concentration distributions with $(N_{\text{air}}, NO_3(1 \pm y_j/2))$, $(N_{\text{air}}(1 \pm z_j/2), NO_3)$ respectively. From Eqs. (5 ~ 10), we obtain:

$$F_i = \left(\sum_{j=1}^{n} D_{ij} y_j + \sum_{j=1}^{n} E_{ij} z_j\right) \varepsilon_i, \quad i = 1, 2, \cdots, m. \tag{12}$$

The above inversion equations are used to get numerical solutions.

1.2.2 Weighting functions and selection of wavelengths. As mentioned above the differential coefficients (E_{ij}, D_{ij}) correspond to the sensitivity of radiance to a relative change of air density and ozone concentration, respectively. The indices i, j correspond to the tangent ray height l_i along the optical axis of the detector and altitude x at which air density and ozone increment are considered, respectively. In present numerical simulation the solar zenith angle is assumed to be 45° and the Air Force Geophysics Laboratory (AFGL) middle latitude summer atmosphere is adopted. In the simulation, two UV wavelengths, i.e. 255 nm and 296 nm, are selected. These two wavelengths represent strong Rayleigh scattering and strong ozone absorption (255 nm), as well as relatively weak Rayleigh scattering and relatively weak ozone absorption (296 nm). The field of view of the detectors is assumed to correspond to 1 km at the limb and the tangent ray height l_i is scanned from 50 km to 100 km in discrete 1-km interval. From Fig. 2 shown below it can be seen that the weighting functions of this limb-scan method are much narrower than those for observations in the satellite nadir direction[1], hence one should be able to determine the vertical air density and ozone distributions above 50 km with a high degree of vertical resolution using the limb-scan method for a double wavelength inversion algorithm at 255 nm and 296 nm.

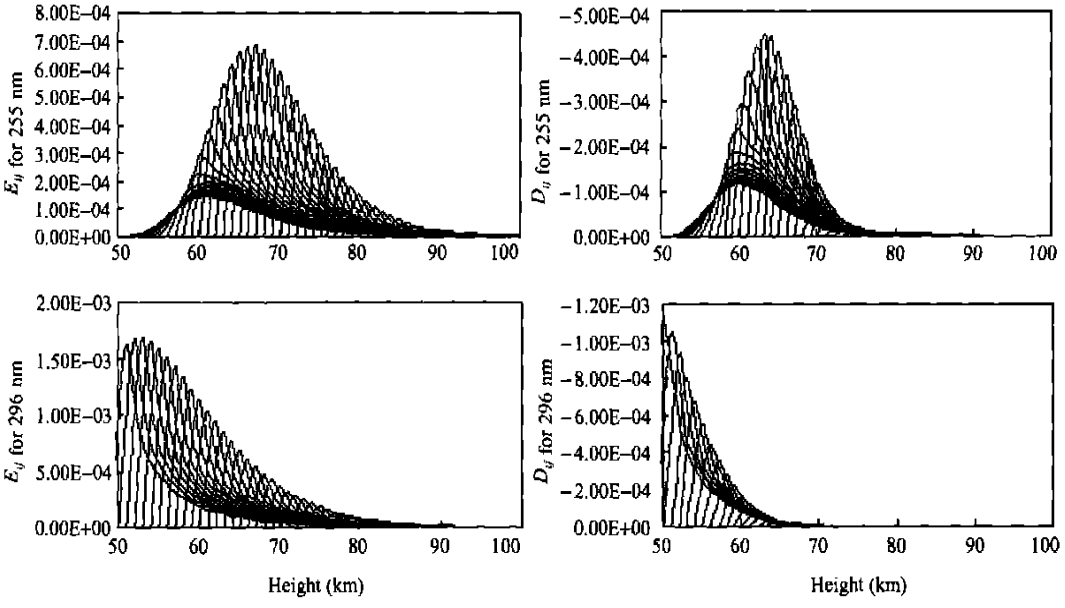

Fig. 2. Differential coefficients E_{ij} for air density and D_{ij} for ozone concentration. The observational tangent ray height is scanned from 50 km to 100 km in discrete 1-km intervals and each line is for one of the observation tangent ray heights.

2 Results

2.1 Numerical simulations

In this section, the results of numerical simulations for determining the vertical distributions of air density and ozone concentration are shown. In the simulations the two wavelengths 255 nm and 296 nm are jointly used to retrieve the air density and ozone vertical distributions in the mesosphere over the 50 km ~ 100 km altitude range, with the interval of 1 km. The atmosphere used is the AFGL middle latitude summer atmosphere. The effects of aerosols are assumed to be negligible for the simulations because

the aerosol optical depth is negligible with respect to the UV Rayleigh optical depth at higher heights above 20 km and of wavelengths shorter than 300 nm. Aerosol effects would be taken into account in multiple-scattering corrections later in retrieving air density and ozone concentration profiles in the lower stratosphere with longer wavelengths larger than 300 nm. In the following we conduct the experiments of joint retrieval (hereafter referred to as JE) for four different cases:

Case 1. The "true" air density and ozone concentration profiles are the pre-determined distributions plus random variations. The limb measurement data are the sum of the model-calculated radiances for the "true" atmosphere and the random observation error. The relative magnitude of random error is $+1.0\%$.

Case 2. The "true" air density and ozone concentration profiles are constructed similar to those of Case 1 while the limb measurement data are of a bias of $+1.0\%$ for both 255 nm and 296 nm.

Case 3. The "true" air density and ozone concentration profiles are constructed similar to those of Case 1, while the limb measurement data are of a bias of -1.0% for both 255 nm and 296 nm.

Case 4. The "true" air density and ozone concentration profiles are the predetermined distribution plus a bias of $+6.0\%$ for air density and -10.0% for ozone concentration while the limb measurement data are of a bias of $+1.0\%$ for both 255 nm and 296 nm. Other parameters for the different cases are the same and unchangeable during the numerical simulation.

In addition to the above-mentioned joint experiments (JE) for each of 4 cases, the other two experiments referred to as single experiments (SE) and ideal single experiments (ISE) are conducted. In the SE, parameters are the same as those of JE except that only the shorter wavelength 255 nm is chosen to infer air density and ozone concentration individually by using the Direct Method proposed by Aruga. In the ISE, parameters are the same as those of SE with an exception that when ozone is retrieved, the true air density profile is assumed to be known and on the contrary, when the air density is retrieved, the ozone concentration profile is known. The ISE is an ideal situation, since in real atmosphere, all parameters are unknown. Fig. 3 shows the results of numerical simulations of four cases.

2.2 Discussions

From all of the eight sub-figures in Fig. 3, it can be clearly seen that the retrieved profiles in JE experiments are much closer to the real ones than those in SE experiments. The inferred SE atmospheric profiles are better than that of predetermined ones in a relative limited height range. To get more clear and quantitative results of the inversion precision, we define an effective inversion height range referred to as EIHR, where the profiles of the inferred atmospheric parameters are much closer to those of the real ones than those of model-estimated ones.

Furthermore, from Fig. 3 one could find that in the SE experiments, the effective inversion height range of air density is almost unanimously from 70 km to 99 km with an exception for the fourth case of an EIHR of 68 to 99 km, while in the JE experiments, the EIHR of air density is from 50 km to 99 km except the first case with an EIHR of 52 km to 99 km; as for ozone density, the EIHR in the SE experiments is nearly the same from 50 km to 68 km, except for the fourth case which has an EIHR between 50 km and 65 km. In the corresponding JE experiments, the EIHR is 50 km to 99 km except that the first case has an EIHR of 52 km to 87 km and the fourth case of 50 km to 95 km. Table 1 shows the EIHR of both air density and ozone concentration for each case in both the SE and JE experiments.

Table 1. EIHR of air density and ozone concentration for each case in SE and JE (unit: km)

Case	EIHR of air density		EIHR of ozone concentration	
	SE	JE	SE	JE
Case 1	70~99	52~99	50~68	52~87
Case 2	70~99	50~99	50~68	50~99
Case 3	70~99	50~99	50~68	50~99
Case 4	68~99	50~99	50~65	50~95

Table 2 shows the corresponding rms (root-mean-square) error in the range of EIHR for four cases in both SE and JE experiments.

Table 2 indicates that in the height range of EIHR, both air density and ozone profile in the SE are much closer to the real ones than those of the predetermined profiles. However, out of the range of EIHR, the inversion precision is low which makes little progress on improving the accuracy of inversion. While in the JE experiments, the inversion precision by joint inversion method is greatly improved com-

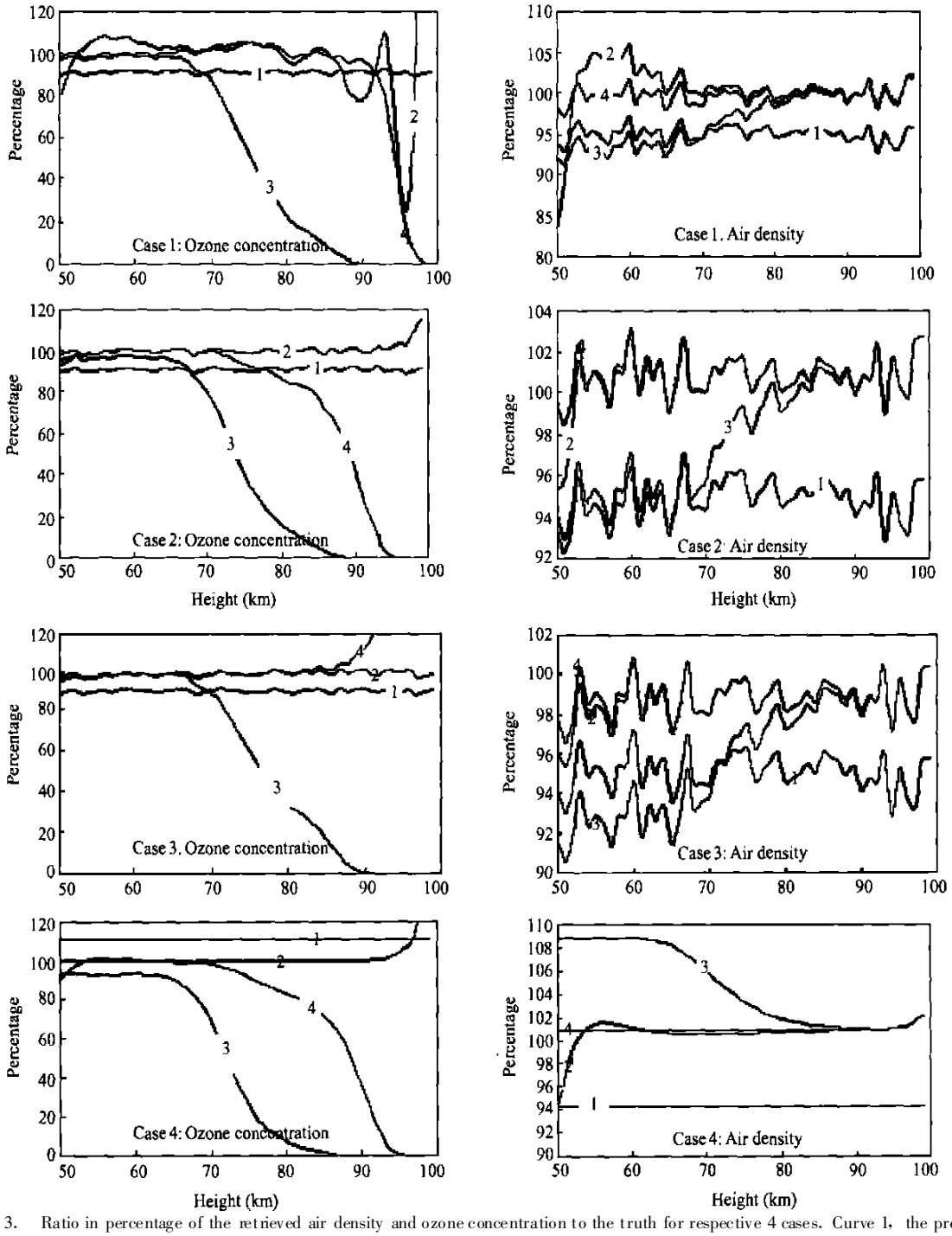

Fig. 3. Ratio in percentage of the retrieved air density and ozone concentration to the truth for respective 4 cases. Curve 1, the pre-determined distribution to the truth; Curve 2, the retrieved distribution to the truth in JE; Curve 3, the retrieved distribution to the truth in SE; Curve 4, the retrieved distribution to the truth in ISE.

pared with that by single inversion method. Here we should point out that among the three kinds of experiments for four cases, profiles by the ideal single inversion method are the closest ones to the real ones but on the risk of sacrificing the range of EIHR especially in the ozone inversion.

Table 2. Average rms errors for air density and ozone concentration in the height range of EIHR (%)

Case	rms error for air density		rms error of ozone concentration	
	SE	JE	SE	JE
Case 1	2.45(4.97)	2.19(4.20)	2.63(9.13)	4.29(9.03)
Case 2	1.53(4.93)	1.58(4.99)	4.56(9.13)	3.11(9.10)
Case 3	2.50(4.93)	1.69(4.99)	1.87(9.13)	1.32(9.10)
Case 4	2.50(5.66)	1.29(5.66)	7.10(11.11)	2.16(11.11)

Note: values in the brackets are the average rms errors for the estimated profiles.

3 Conclusion

The joint method for inferring the vertical air density and ozone distributions in the mesosphere on a global basis from satellite observation is described in this paper. In this method, the observation from a spacecraft is made in such a way that the scattered solar UV radiation is observed as a function of the height of the tangent ray at the limb of the atmosphere. The authors give four examples of different kinds of parameter setting. From the analysis shown above, one may draw the following conclusions.

(i) The joint retrieval method is feasible and gives better results than those of single retrieval algorithm with similar parameters.

(ii) The JE is of higher accuracy of air density and ozone concentration inversion, that is, the inversion errors of air density and ozone concentration are greatly decreased through the whole targeted height range as well as that the JE retrieves ozone concentration effectively to a higher altitude up to more than 95 km while the SE has an effective height range of 50 km ~ 70 km of satisfactory inversion outcome.

(iii) The present joint retrieval method can be extended to the stratosphere by using longer wavelengths provided that the corrections of multiple scattering and the contribution of aerosols are taken into account. This is our future work.

References

1 Bhartia, P. et al. Algorithm for the estimation of vertical ozone profiles from the backscattered ultraviolet technique. J. G. R., 1996, 101: 18793.

2 Rusch, D. W. et al. Solar mesosphere explorer ultraviolet spectrometer: measurement of ozone in the 1. 0 ~ 0. 1 mbar region. J. Geo. Res., 1984, 89(7): 11677.

3 Barch, C. A. et al. Solar mesosphere explorer: scientific objectives and results. Geo. Res. Lett., 1983, 10: 237.

4 Rusch, D. W. et al. Ozone densities in the lower mesosphere measured by a limb scanning ultraviolet spectrometer. Geo. Res. Lett., 1983, 10: 241.

5 Thomas, R. J. et al. Ozone density distribution in the mesosphere (50 ~ 90 km) measured by the SME limb scanning near infrared spectrometer. Geo. Res. Lett, 1983, 10: 245.

6 Thomas, R. J. et al. Mesospheric ozone depletion during the solar proton event of July 13, 1982. Part I. Measurement. Geo. Res. Lett, 1983, 10: 253.

7 Solomon, S. et al. Mesospheric ozone depletion during the solar proton event of July 13, 1982. Part II. Comparison between theory and measurements. Geo. Res. Lett., 1983, 10: 257.

8 Flittner, D. E. et al. O_3 profiles retrieved from limb scatter measurements: Theory. Geophys. Res. Lett., 1999, 27: 2601.

9 McPeters, R. D. et al. The retrieval of ozone profiles from limb scatter measurements: results from the shuttle ozone limb sounding experiment. Geophys. Res. Lett., 2000, 27: 2597.

10 Tadashi Aruga et al. Vertical distribution of ozone: a new method of determination using satellite measurements. Appl. Opt., 1976, 15(1): 261.

11 Tadashi Aruga et al. Determination of vertical ozone distributions by spacecraft measurements using a limb-scan technique. Appl. Opt., 1982, 21(16): 3047.